China Ocean Eng., 2022, Vol. 36, No. 5, P. 781–790
DOI: https://doi.org/10.1007/s13344-022-0069-9, ISSN 0890-5487
http://www.chinaoceanengin.cn/ E-mail: coe@nhri.cn

Shear Strength and Dilatancy of Calcareous Sand in the South China Sea

PEI Hui-min[a], WANG Dong[a, b, *]

[a] Shandong Provincial Key Laboratory of Marine Environment and Geological Engineering, Ocean University of China, Qingdao 266100, China

[b] Qingdao National Laboratory for Marine Science and Technology, Qingdao 266100, China

Received August 13, 2021; revised June 16, 2022; accepted July 12, 2022

Abstract

The shear strength and dilatancy of typical uncemented calcareous sand from the South China Sea are investigated by soil lab tests. According to drained triaxial tests at various relative densities and confining stresses, it is found that the constant volume friction angle is approximated as 39° and the traditional Bolton's equations can be modified to estimate the peak friction angle and dilation angle. The reliability of the equation proposed for the peak friction angle is verified in terms of calcareous sands from more onshore and offshore sites worldwide, while the errors of the predicted dilation angles scatter in a relatively large range. Totally, the dilation angles of sands in the South China Sea are estimated by the equation presented with an error of ±30%. The peak friction angle measured by the undrained is similar to that by the drained tests as the relative density smaller than 60%, while the former is slightly lower for denser samples.

Key words: calcareous sand, triaxial tests, friction angle, dilatancy, drained, South China Sea

Citation: Pei, H. M., Wang, D., 2022. Shear strength and dilatancy of calcareous sand in the South China Sea. China Ocean Eng., 36(5): 781–790, doi: https://doi.org/10.1007/s13344-022-0069-9

1 Introduction

Calcareous sand is widely distributed on coral reefs and seashores around the world such as the South China Sea, North-West shelf of Australia, Red sea and Bass Strait. The strength or deformation behaviors of calcareous sands are distinguished from silica sands due to their fundamental differences on the shape and mineral of soil particles, the cementation and inner pore, as reported by Lee and Poulos (1991), Airey (1993), Erbrich et al. (2010) and Wang et al. (2017) among others. Additionally, the physical and mechanical properties of calcareous sand were formed further by offshore hydrodynamics environment. Shallow footings, piles and spudcan footings used in nearshore or offshore constructions may be installed on calcareous sands (Cassidy et al., 2005; Lehane et al., 2012). For offshore and coastal practical applications between latitudes 30°N and 30°S, calcareous sands might be potentially employed as hydraulic filling material in constructions of harbors (He et al., 2020), road embankments and airport runways (Wang et al., 2017). It was found that the bearing capacity of shallow footing on calcareous sand was higher than that on silica sand due to the higher small-strain stiffness and strength of calcareous sand (Wang et al., 2011).

The strength and dilatancy of both the silica sands and calcareous sands can be interpreted through the internal friction angles and dilation angles. It is already recognized that the internal friction angle of sand is the function of mineralogy and the appearances of mica and calcite materials (Bolton, 1986), while Liu and Lehane (2012) reported that the constant volume friction angle φ'_{cv} and peak friction angle φ'_{p} reduce approximately linearly with the particle regularity. The calcareous sands may be naturally cemented owing to the process of deposition. The particles breakage may occur during shearing (Coop, 1990), which complicates the interpretation of triaxial test results. However, the cementation and particle breakage are negligible in a number of calcareous sand types, such as those at Ledge Point and Kwinana in Australia (Teng et al., 2020; Jensen, 2018) and in a few regions in the South China Sea (Rui et al., 2020). For silica sands, the internal friction angles and dilation angle are dominated by the relative density I_D and the stress level, while the cementation and particle breakage can be ignored reasonably in most cases. Bolton (1986) suggested the following equations to estimate φ'_{p} and the peak dilation angle ψ_p

$$I_R = I_D(Q - \ln p'_p) - R; \tag{1}$$

$$\varphi'_p - \varphi'_{cv} = mI_R; \tag{2}$$

Foundation item: This work is financially supported by the National Natural Science Foundation of China (Grant Nos. U1806230 and 42025702).
*Corresponding author. E-mail: dongwang@ouc.edu.cn

$$\varphi'_{\mathrm{p}} - \varphi'_{\mathrm{cv}} = 0.8\psi_{\mathrm{p}}, \quad (3)$$

where I_{R} is the relative dilatancy index, p'_{p} is the mean effective stress at peak strength and Q, R and m are empirical parameters. Bolton (1986) suggested the typical value for φ'_{cv} as 33° for silica sand, and Q = 10, R = 1 and m = 3 were fitted to estimate φ'_{p} and ψ_{p} under triaxial strain. The robustness of Eqs. (1)–(3) has been proved through a large quantity of tests during the last three decades, although the values of φ'_{cv} and the empirical parameters may vary with the types of sand. For example, the φ'_{cv} values of silica sands ranged between 29° to 33° in Bolton (1986), Negussey et al. (1988), Jamiolkowski et al. (2003) and Andersen and Schjetne (2013). The value of Q, depending on the mineralogy and shape of soil particles, is decreased with increasing compressibility of particles, i.e. lower Q for soils with weaker grains (Bolton, 1986; Jamiolkowski et al., 1988).

It is not clear if Eqs. (1)–(3) can be expanded to calcareous sands, since the mineralogy and shape of grains of calcareous sands distinguish remarkably from those of silica sands. Although a large quantity of experimental studies were carried out to investigate the strength and deformation of calcareous sands as summarized by Coop (1990), Airey (1993), Kuwajima et al. (2009) and Wang et al. (2020), the attempts to establish a simple relationship similar to Eqs. (1)–(3) are very limited. An exception is by Jamiolkowski et al. (2003) who suggested Q = 9.5 and Q = 7.5 for two calcareous sands, Kenya sand and Quiou sand, respectively.

In this paper, a total number of 51 triaxial compression tests in terms of uncemented calcareous sand from the South China Sea are conducted, and the empirical equations for estimating the internal friction angles and dilatancy of this regional calcareous sand are proposed by modifying the classic Bolton's equations. The modified equations are testified further through comparison with the existing triaxial tests of calcareous sands from a few onshore and offshore sites worldwide.

2 Sample and testing procedure

The soil sample used was calcareous sand from the South China Sea, and the content of $CaCO_3$ was up to 90% in weight (Wang et al., 2017). Samples of calcareous sand were obtained from a lagoon on a coral reef. According to Xiao et al. (2018) and Lv et al. (2020), the particles larger than 2 mm were screened out to avoid the particle size effect. The initial grain size distribution (GSD) curve prior to the triaxial tests is shown in Fig. 1. The particles finer than 0.075 mm account for 16% of the total particles for sample.

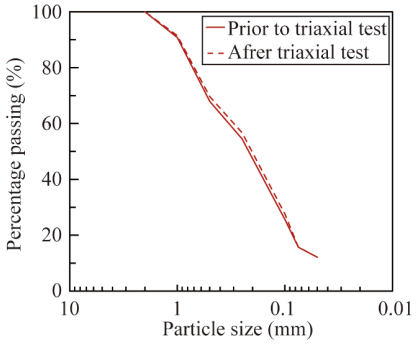

Fig. 1. Grain size distribution curves.

The physical properties were measured as: the maximum void ratio $e_{\max}$ = 1.33, the minimum void ratio $e_{\min}$ = 0.60 and the specific gravity G_{s} = 2.80. The specific gravity of calcareous sand reported by literature varies over a wide range from 2.68 to 2.86 (see Table 1). A possible reason is that the carbonate content of calcareous sand varied with sites. In addition, we found that the value of G_{s} depends on the boiling or pumping method used. For samples studied here, G_{s} was measured as 2.73 through the pumping method, while G_{s} = 2.80 through the boiling method. As the calcareous sand is with abundant pores, the boiling method is preferred to determine G_{s}.

Fig. 2 shows the scanning electron microscope (SEM) images of particles at 1000 and 8000 magnifications. The sand samples studied were from an island in the South China Sea, without undergoing long-distance movements during depositing. Therefore, the particles are moderately irregular in shape, and the rod-like, rounded, block and column particles are observed in Fig. 2a. The particles consist of mainly the remains of marine organisms. Similar particle shape was found in the SEMs of calcareous sands from other locations at the South China Sea (Wang et al., 2020; Lu et al., 2000) and from the Kish Island (Hassanlourad et al., 2008). Formed in different offshore hydrodynamics environments, the sand samples studied are distinguished from the offshore or coastal calcareous sands such as the Dog's Bay sand (White and Bolton, 2004) and Goodwyn sand (Sharma and Ismail, 2006). The image with a higher

Table 1 Specific gravities of calcareous sands reported publicly

Regions	G_{s}	References	Regions	G_{s}	References
Hormuz	2.73	Jafarian et al. (2018)	South China Sea	2.81	Rui et al. (2020)
North coast	2.79	Salem et al. (2013)	South China Sea	2.78	Wang et al. (2019)
Cabo Rojo	2.86	Salem et al. (2013)	South China Sea	2.74	Wang et al. (2021)
Playa Santa	2.75	Salem et al. (2013)	South China Sea	2.79	Xiao et al. (2018)
Dogs Bay	2.75	Salem et al. (2013)	South China Sea	2.68−2.78	Wang et al. (2017)
Ewa Plains	2.72	Salem et al. (2013)	South China Sea	2.81	Lv et al. (2020)

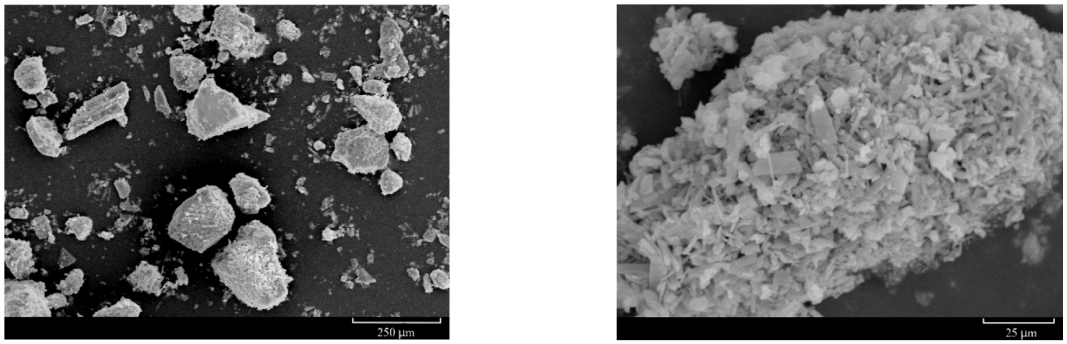

(a) Magnify 1000 times (b) Magnify 8000 times

Fig. 2. Scanning electron microscope images of calcareous sand in the South China Sea.

magnification (in Fig. 2b) reveals a rough particle surface with finer particles attached, which may be attributed to their sedimentary environment in the lagoon.

A total number of 51 triaxial compression tests under drained or undrained conditions were conducted to investigate the shear strength and dilatancy of the calcareous sand. The samples with diameter of 50 mm and height of 100 mm were prepared in a three-flap mold. A 0.3 mm-thick rubber membrane was used, and the dried sand was spread in five separate layers into the mold. No high-energy hammering was allowed in sample preparation, to avoid unexpected particle breakage. Salem et al. (2013) reported that it is difficult to achieve full saturation of the sample, due to the abundant pores of calcareous sands. Here, a combination of water saturation, carbon dioxide saturation, and back pressure saturation was thus conducted to guarantee the saturation. The water in pipe needs to be emptied before carbon dioxide (CO_2) passed through, which will speed up the saturation. After about 20 min of passing CO_2, the de-aired water was driven through from the bottom of the sample until the gas in sample was emptied sufficiently. Then a backpressure less than 300 kPa with a confining stress σ'_3 of 20 kPa was applied on samples to saturate it further. As the sample was saturated by carbon dioxide, de-aired water and back pressure, the B values in all triaxial tests were no less than 0.95, suggesting that the sample was nearly saturated.

The sample were isotropically consolidated under the confining stress of 50−800 kPa and the relative density of samples prior to shearing ranged from 41% to 91%. To explore the potential of particle breakage, the GSD curves prior to and after the triaxial tests were obtained by sieving tests. An example is shown in Fig. 1: for a triaxial test with I_D = 80.7% and σ'_3 = 600 kPa, the peak deviatoric stress was as high as 2823 kPa and the corresponding mean effective stress was 1540 kPa. The GSD curve was nearly unchanged after shearing, suggesting that the particle breakage was slight.

The axial strain was measured as $\varepsilon_a = \Delta h/h$, where Δh and h were the change of sample height and the height of sample after consolidation, respectively. Correspondingly, the volumetric strain $\varepsilon_v = \Delta V/V$, where ΔV and V are the change of volume and the volume of sample after consolidation. φ'_{cv} was defined as the angle when the sample is at constant volume or constant deviatoric stress. The volumetric strain versus axial strain plot was used as a criterion to define the critical state. On some occasions, the volume strain is changed slightly or moderately, but the deviatoric stress remains constant. By following Salgado et al. (2000), Been and Jefferies (2004) and Carraro et al. (2009), it is recognized that the critical state is reached. The internal frictional angle φ' and peak dilation angle ψ_p in triaxial compression tests are determined by

$$\sin\varphi' = \frac{3\eta}{6+\eta}; \tag{4}$$

$$\sin\psi_p = -\frac{\left(\dfrac{d\varepsilon_1}{2d\varepsilon_3}\right)_{max}+1}{\left(\dfrac{d\varepsilon_1}{2d\varepsilon_3}\right)_{max}-1}, \tag{5}$$

where $d\varepsilon_1$ and $d\varepsilon_3$ are principal strain increments; the stress ratio $\eta = q/p'$, q and p' denote the deviatoric stress and mean effective stress, respectively.

3 Empirical equations to estimate φ'_p and ψ_p of calcareous sand

As shown in Table 2, 39 triaxial compression drained tests were conducted to obtain the empirical equations to estimate φ'_p and ψ_p of calcareous sand. Typical q−ε_a and ε_v−ε_a curves obtained are shown in Fig. 3. Strain-softening was observed in most tests, but the axial strain corresponding to the peak deviatoric stress was dependent on the relative density and confining stress. With the increase of relative density or decrease of confining stress, the axial strain at the peak deviatoric stress decreases. By comparing the stress−strain curve and the volume strain response, it is found that the peak deviator stress and the peak rate of volumetric strain to axial strain appear almost at the same time. It means that the mobilization of maximum strength is accompanied by maximum dilatancy. The volume of all samples are contracted at the early stage of shearing, followed

Table 2 Drained triaxial test results

Test No.	I_D (%)	σ'_3 (kPa)	p'_p (kPa)	Measured φ'_p (°)	Measured φ'_{cv} (°)	Measured ψ_p (°)	Predicted φ'_p (°)	Predicted ψ_p (°)
1	43.2	80	189	43.1	39.4	6.2	45.1	3.0
2	46.0	200	487	43.4	37.9	4.4	43.8	5.9
3	47.6	200	514	44.6	39.6	4.7	43.9	5.0
4	47.9	50	128	45.1	38.5	8.9	46.5	8.0
5	48.2	150	369	43.8	39.7	4.4	44.6	3.6
6	48.8	120	293	42.9	38.4	4.8	45.1	4.2
7	49.2	400	995	43.7	39.3	2.8	42.7	4.1
8	50.8	300	751	43.6	39.6	2.8	43.4	3.5
9	50.8	180	451	43.8	39.4	4.2	44.5	4.1
10	51.2	300	748	43.8	40.4	2.7	43.5	2.6
11	51.4	300	753	44.0	39.9	4.2	43.5	3.6
12	52.8	400	984	43.4	39.0	3.9	43.1	4.1
13	53.1	600	1436	42.6	37.9	2.5	42.3	4.5
14	53.3	50	138	46.8	38.8	12	47.3	11.0
15	55.7	150	382	44.4	38.3	6	45.4	7.0
16	58.0	150	393	45.1	40.0	6.8	45.6	5.2
17	60.6	100	274	46.3	39.8	8.1	46.8	7.8
18	61.0	200	543	45.5	39.1	6.8	45.2	7.6
19	61.5	200	511	44.4	39.8	6.9	45.4	4.4
20	63.7	200	541	45.5	39.6	6.4	45.5	6.6
21	64.3	300	754	44.0	39.4	3.8	44.7	4.4
22	64.3	400	1005	44.0	38.8	3.7	44.0	5.4
23	64.5	500	1216	43.0	39.4	3.5	43.5	2.9
24	67.0	100	306	48.3	39.3	11.8	47.4	13.4
25	68.3	230	634	46.6	39.9	6	45.6	8.2
26	73.4	60	211	51.7	40.0	17.9	49.3	11.7
27	73.8	80	221	47.8	39.5	14.0	49.2	9.6
28	74.2	300	829	46.5	39.3	7.9	45.4	9.2
29	75.4	200	579	47.5	38.0	11	46.6	14.6
30	77.3	400	1076	45.9	38.5	7.2	44.8	8.8
31	77.4	180	535	48.3	39.9	9.7	47.0	9.9
32	77.6	200	567	47.0	38.8	10	46.9	11.4
33	79.3	300	804	45.8	38.0	6.8	45.9	10.3
34	79.5	100	311	49.5	39.4	13.1	49.0	16.2
35	80.7	600	1540	44.6	38.4	5.4	44.0	7.2
36	82.9	80	272	51.2	38.6	19.6	49.9	23.4
37	86.4	375	1088	47.6	38.8	10	45.5	12.9
38	86.5	150	429	47.6	40.0	11.5	48.8	10.8
39	89.4	400	1150	47.5	38.2	9.4	45.6	13.1

by dilation. The dilatancy of calcareous sand is increased significantly with increasing relative density and decreasing confining stress: the sample with I_D = 79.5% and σ'_3 = 100 kPa shows dilatancy, whilst the other three samples are in a tendency of volume contraction. In addition, the axial strains corresponding to the peak deviatoric stress of calcareous sand are obviously larger than those of silica sands. For example, the axial strain in terms of the peak deviatoric stress reaches ~6.1% in Test 34 with I_D = 79.5% and σ'_3 = 100 kPa. Under the similar relative densities and confining stresses, the axial strain of Ottawa sand, a type of silica sands used extensively, was reported as ~3% by Salgado et al. (2000), ~2% by Guo and Su (2007) and ~3.5% by Carraro et al. (2009). The larger axial strain at peak stress may be attributed to the irregular particle shapes of calcareous sands judging from the SEM (see Fig. 2): the angularity of particles causes more substantial interlocking that restrains sliding and rotation between particles, the larger axial strain is thus required to mobilize the peak deviatoric stress.

The influences of p'_p and I_D on φ'_{cv} are illustrated in Fig. 4, in which the influences can be neglected reasonably and it is approximated as φ'_{cv} = 39° for the samples studied. The values of φ'_{cv} and φ'_p reported by Coop (1990), Coop and Atkinson (1993), Lehane et al. (2014) and Airey (1993) are listed in Table 3. Most of the calcareous sands from different regions at various stress levels are featured with φ'_{cv} varying between 38° and 45°. Liu and Lehane (2012) found the dependence of φ'_{cv} on particle shape and the φ'_{cv} value tends to decrease with increasing particle regularity. The particle shape of calcareous sand may vary with the site,

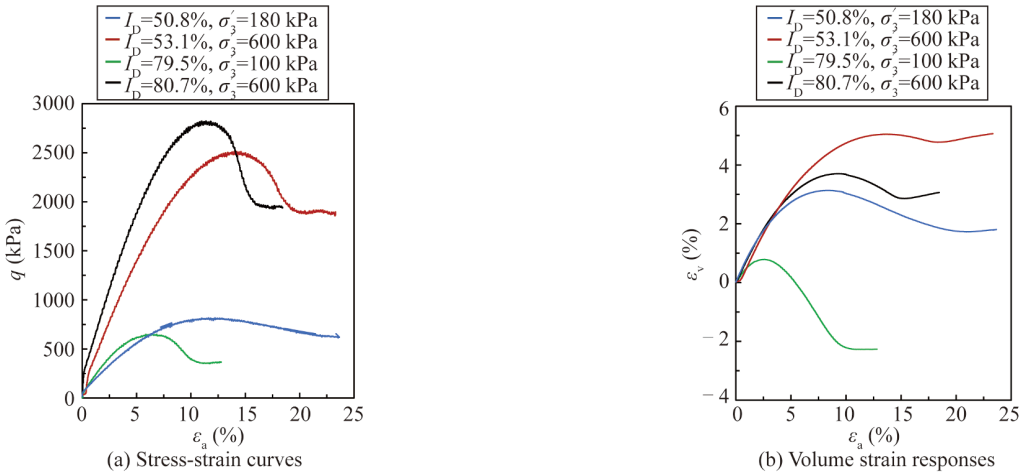

(a) Stress-strain curves (b) Volume strain responses

Fig. 3. Typical results of drained triaxial tests.

(a) φ_{cv}' as a function of p_p' (b) φ_{cv}' as a function of I_D

Fig. 4. Constant volume friction angles measured.

which leads to the scattered values of φ'_{cv}. Overall, the range of φ'_{cv} measured here is consistent with those around the world. Compared with the silica sand, calcareous sand has different mineral composition, more irregular particle shape and rougher surface. Obviously, φ'_{cv} of calcareous sand is much higher than those of most silica sands ranging from 29° to 33° reported by Bolton (1986), Negussey et al. (1988), Jamiolkowski et al. (2003) and Andersen and Schjetne (2013).

Based on the drained triaxial tests of the South China Sea sand in Table 2, Bolton's empirical Eqs. (1)–(3) are followed but the values of Q, m and R need to be modified. By least-square fitting, the parameters are determined as $Q = 9$, $R = 0.1$ and $m = 4$, therefore,

$$I_R = I_D\left(9 - \ln p'_p\right) - 0.1; \tag{6}$$

$$\varphi'_p - \varphi'_{cv} = 4I_R. \tag{7}$$

Compared with silica sands, the higher value of m and lower value of R indicate that the divergence between φ'_{cv} and φ'_p is more remarkable for calcareous sand tested. It refers to the fact that the level of dilatancy during shearing is higher. The Q value fitted is lower than $Q = 10$ for silica sands, indicating that the calcareous sand has higher compressibility. This is consistent with the findings by Bolton (1986) and Jamiolkowski et al. (2003). Fig. 5 shows the relationship between $(\varphi'_p - \varphi'_{cv})$ and p'_p under different values of I_D. The experimental data of $(\varphi'_p - \varphi'_{cv})$ agree well with the predictions by Eq. (7) with typical I_D of 40%, 60%, 75% and 90%. The values of φ'_p measured and predicted are scattered within a narrow discrepancy of ±5%, as p'_p = 128–1540 kPa and I_D = 40%–90%.

A power function is presented to calculate ψ_p of the cal-

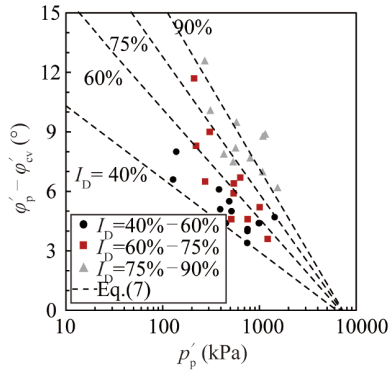

Fig. 5. Variation of $(\varphi'_p - \varphi'_{cv})$ with p'_p under different I_D.

careous sand samples

$$\varphi'_{\mathrm{p}} - \varphi'_{\mathrm{cv}} = 1.9\psi_{\mathrm{p}}^{0.6}. \quad (8)$$

The dilation angle is closely related to the particle rolling and rearrangement. Therefore, the particle shape has a crucial influence on the dilatancy. Eq. (8) for calcareous sand is obviously varying from Eq. (3) for silica sands, which can be attributed to the irregular particle shapes of calcareous sand (see Fig. 2). Compared with the traditional linear relationship in Eq. (3), the power function is more suitable to describe the dilatancy of calcareous sand in the South China Sea. The predictions of ψ_{p} by Eq. (8) are compared with the measured in Fig. 6, and the maximum error approaches ±30%. However, the maximum divergence is 3.8°, and more than 80% of predictions lie within a divergence of 2°. The prediction deviation of Eq. (8) for dilation angle is acceptable. In fact, the prediction of dilatancy angle in Eqs. (1)–(3) is not as accurate as that of the peak internal friction angle. Note that Eqs. (6)–(8) are applicable to p'_{p} ranging from 100 kPa to 1600 kPa. Currently, we are not sure if the equations can be extended to higher stress levels, since the higher stress may result in particle breakage. The empirical equations are fitted in terms of calcareous sand with negligible particle breakage.

4 Reliability of empirical equations

Eqs. (6)–(8) are based on the triaxial data of the samples from a specific location in the South China Sea. To testify the reliability and robustness of the equations, the equations and the suggested values of Q, R and m are employed to predict φ'_{p} and ψ_{p} of uncemented calcareous sands sampled worldwide (Table 3). Based on the stress-strain curves and volume strain response reported publicly, the deviator stress $q = \sigma'_1 - \sigma'_3$ and the value of $\mathrm{d}\varepsilon_1/\mathrm{d}\varepsilon_1$ can be obtained. Then, the mean effective stress, internal frictional angle and peak dilation angle are determined by Eqs. (4) and (5). Severe particle breakage was observed in the triaxial tests for sands from Dogs Bay and Ballyconneely, while the breakage is slight in sands from the South China Sea, Kish Island, Tonbak, Hormuz Island and Bushehr Port. The carbonate contents are at least 91%, except for 54% for the Hormuz Island sand and 45% for Bushehr Port sand (Rezvani, 2020). The value of φ'_{cv} used for the prediction by Eqs. (6)–(8) is obtained by the measurement in triaxial tests and it varies with the location of sand.

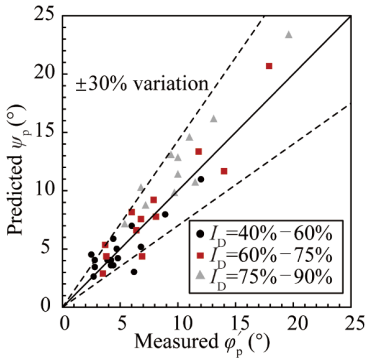

Fig. 6. Comparison of peak dilation angles predicted and measured.

Table 3 Ranges of φ'_{cv} and φ'_{p} for different calcareous sands

Soil	Region	Confining stress (kPa)	φ'_{cv} (°)	φ'_{p} (°)	Degree of breakage	Reference
Dogs Bay sand	The west of Ireland	50−7500	40	N/A	Severe	Coop (1990)
Dogs Bay sand	The west of Ireland	150−12120	37(artificially) 39(natural)	N/A N/A	N/A	Coop and Atkinson (1993)
Dogs Bay sand	The west of Ireland	100−1000	38−49.8	38−52.2	N/A	Golightly and Hyde (1988)
Dogs Bay sand	The west coast of Eire	50−400	38−43	38−49	Severe	Kuwajima et al. (2009)
Dogs Bay sand	The west of Ireland	100 1000	40 38	47 38	Severe	Doherty et al. (2016)
South China Sea sand	The South China Sea	50−300	40−46	45−62.5	N/A	Wang et al. (2019)
South China Sea sand	The South China Sea	50−400	39.7	42.7−52.5	Slight	Wang et al. (2020)
South China Sea sand	The South China Sea	100−1600	40.4−43.6	40.4−51.4	Slight	Wu et al. (2020)
South China Sea sand	The South China Sea	300−800	32.8−40.9	38.4−46.4	Slight	Zhang and Luo (2020)
Carbonate sand	The North−West shelf of Australia	600−700	37−45	N/A	N/A	Airey (1993)
Ballyconneely sand	Ballyconneely Bay of Ireland	100 1000	39 35	43 35	Severe	Doherty et al. (2016)
Chiibishi sand	Okinawa in Japan	100−400	44	44−50	N/A	Kuwajima et al. (2009)
NWS silty sand	The North−West shelf of Australia	N/A	37.8−38.8	N/A	N/A	Lehane et al. (2014)
Kish Island sand	Persian Gulf in the south of Iran	50−600	39.7−41.1	40.4−46.9	Slight	Hassanlourad et al. (2008)
Tonbak sand	Persian Gulf in the south of Iran	50−600	39.1−42.2	39.2−45.3	Slight	Hassanlourad et al. (2008)
Hormuz Island sand	The north coast of the Persian Gulf	100−600	35.3−39.7	36.7−45.1	Slight	Rezvani (2020)
Bushehr Port sand	The north coast of the Persian Gulf	100−600	31.5−37	31.5−41.6	Slight	Rezvani (2020)
Red Sea sand	The Red Sea	100−300 300−1000	42 37	49 42	N/A	Baghdadi et al. (1991)

(1) As shown in Fig. 7a, φ'_p is estimated well by Eq. (7) for calcareous sands from other locations at the South China Sea (Wang et al., 2019, 2020; Wu et al., 2020; Zhang and Luo, 2020) and the Red Sea (Baghdadi et al., 1991), the Kish Island and Tonbak (Hassanlourad et al., 2008). Totally, the particle breakage is slight in these sands.

(2) For the calcareous sands at Dogs Bay (Golightly and Hyde, 1988; Kuwajima et al., 2009; Doherty et al., 2016) and Chiibishi (Kuwajima et al., 2009), severe breakage of irregular particles occurred during shearing. The values of φ'_p measured are moderately lower than that predicted by Eq. (7), as demonstrated in Fig. 7b. Daouadji and Hicher (2010) summarized three modes of particle breakage, i.e. fracture, attrition and abrasion. Irregular particles are produced if the fracture mode is dominant, whereas the rupture of sharp angles is caused by the other two modes. Wang et al. (2021) found that the breakage of their calcareous sand sample was dominated by the corner breakoff and surface asperity abrasion during triaxial compression under 400 kPa confining stress. The particle breakage is followed by grinding coarse grains to generate finer particles, then the irregular particles in Fig. 2a becomes more round in shape. Therefore, the relative dilatancy index and peak friction angle are overestimated by Eqs. (6) and (7), given that the calcareous sands are sheared with severe particle breakage.

(3) The Ballyconneely sand is characterized by large round particles, but the hollow grain structures result in particle breakage during shearing (Doherty et al., 2016) and then the measured φ'_p is lower than the prediction by Eq. (7) (see Fig. 7b). The reason of overestimation is similar to that of sands with severe particle breakage.

(4) The carbonate contents of sands from the Hormuz Island and Bushehr Port were as low as 54% and 45%, respectively (Rezvani, 2020). When the equations for silica sand (Bolton, 1986; Salgado et al., 2000) are used to estimate φ'_p, their performances are even better than Eq. (7), as shown in Fig. 7c. It suggests that the strength behavior of Hormuz Island sand and Bushehr Port sand is close to silica sands rather than calcareous sands with carbonate contents higher than 90%.

The dilatancy properties of calcareous sand varied with sites. Eq. (8) is obtained by fitting data of calcareous sand in the South China Sea, and the maximum error approaches ± 30%. The predictions of dilation angle for calcareous sands from other locations are with lower accuracy. When the values of φ'_p and φ'_{cv} listed in Table 3 are known, the ψ_p values can be estimated by Eq. (8). The ψ_p values estimated and measured are compared in Fig. 8. For calcareous sand from the other sites in South China Sea (Wang et al., 2019, 2020; Wu et al., 2020; Zhang and Luo, 2020), the deviation between the measured and predicted values of ψ_p is large but acceptable. For other sands, the values of ψ_p are usually underestimated by Eq. (8) with a considerable deviation. The large divergence is partly due to the differences of particle shape, breakage degree, compressibility and carbonate content.

5 Peak friction angles in the undrained triaxial tests

As listed in Table 4, 12 triaxial compression undrained tests were carried out to obtain the peak friction angles, with the confining stress varying between 100 kPa and 800 kPa and the relative density varying between 41% and 91%. The typical q–ε_a, u_w–ε_a and q–p' curves are demonstrated in Fig. 9, where u_w refers to the excess pore pressure. The peak deviator stress is mobilized at axial strain of 11%–14% (see Fig. 9a), which is much higher than that required for silica sands. In Fig. 9b, the excess pore pressure increases at early stage of shearing and then decreases with the increasing axial strain. The initial contractive tendency and then dilatant tendency of both loose and dense samples are captured by the increased and decreased excess pore pressure, respectively. The different degrees of dilatancy are observed in loose and dense samples. For the sample with confining stress of 600 kPa and relative density of 41%, the maximal u_w reaches 430 kPa. For the sample with I_D = 85% and σ'_3 = 100 kPa, the peak value of u_w is only 50 kPa, followed by a reduction to −300 kPa at 15% axial strain. It means that the sample with low confining stress and high relative density has more dilatant response rather than contractive response.

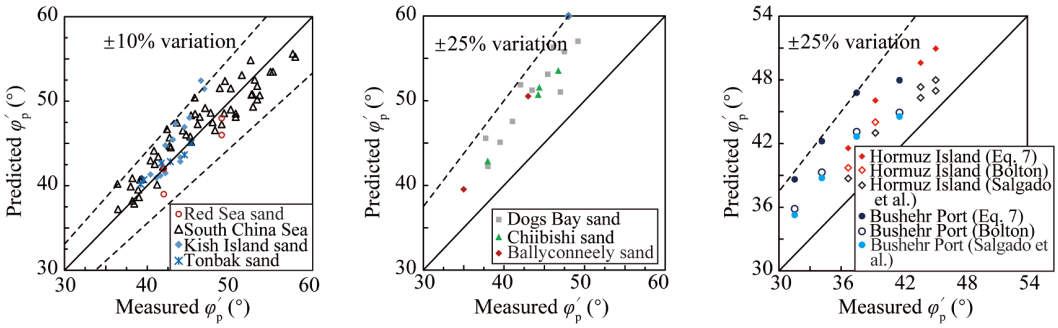

(a) Sands from the South China Sea, the Kish Island, the Tonbak and the Red Sea

(b) Sands from Dogs Bay, Chiibishi and Ballyconneely

(c) Sands from the Hormuz Island and Bushehr Port

Fig. 7. Predictions of peak friction angles for calcareous sands from other locations.

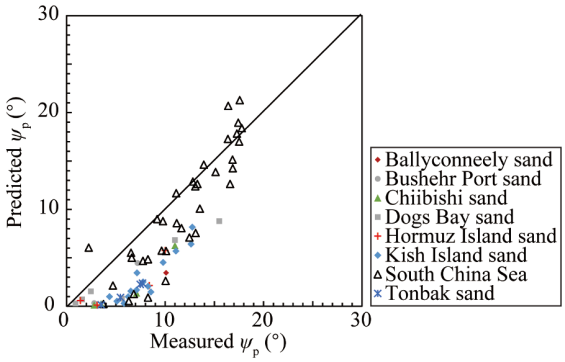

Fig. 8. Predictions of peak dialtion angles for the existing triaxial tests.

Table 4 Undrained triaxial test results

Test No.	I_D (%)	σ'_3 (kPa)	Measured φ'_p (°)
40	41.0	600	42.6
41	43.1	100	43.5
42	47.8	200	42.0
43	44.9	400	44.9
44	59.3	400	45.5
45	77.1	400	45.3
46	81.3	800	45.1
47	83.3	600	46.0
48	85.2	100	48.0
49	88.2	300	46.6
50	88.2	800	47.2
51	90.5	400	47.1

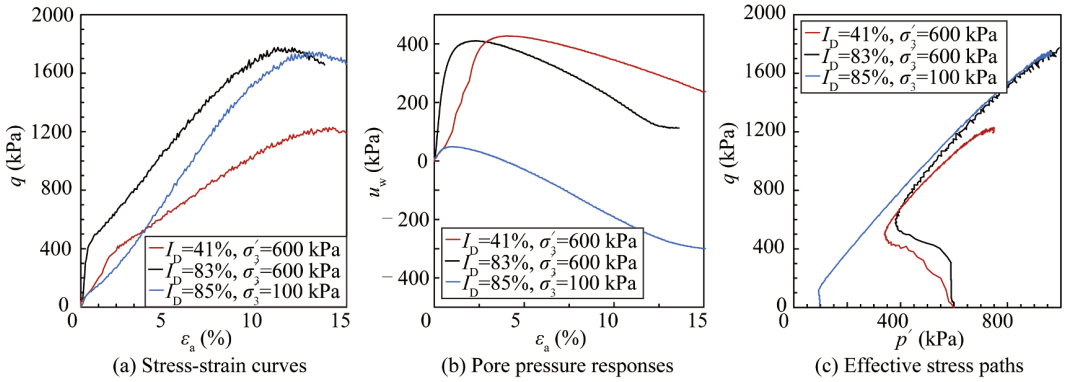

Fig. 9. Typical results of undrained triaxial tests.

In addition, the axial strain corresponding to the initially dilatant tendency is smaller for denser sample, while the effect of the confining stress on the corresponding strain is negligible. Even though the tests were conducted under different confining stresses and relative densities, the effective stress-paths show a similar pattern of behavior in Fig. 9c. All the stress paths fall along straight lines that are almost parallel at the later stages of shearing tests. The responses in undrained triaxial tests are similar to that in monotonic simple shear tests illustrated by Porcino et al. (2008) and Salem et al. (2013).

The values of φ'_p ranged from 42° to 48° in the undrained tests, and the peak friction angles from all drained and undrained tests are compared in Fig. 10. The φ'_p values by drained and undrained tests are close to each other as $I_D < 60\%$, while φ'_p from the drained tests are slightly larger than the companion from undrained tests as $I_D > 60\%$. Andersen and Schjetne (2013) reported that for most silica sands, the measured values of φ'_p in the drained tests are higher. As shown in Fig. 10, φ'_p increased with relative density and decreased with stress level in both drained and undrained tests.

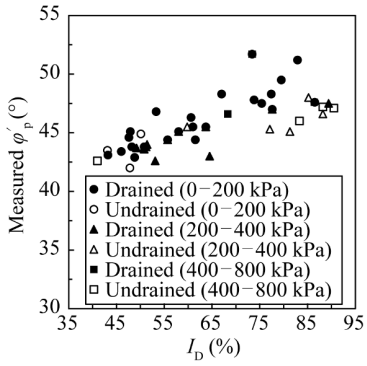

Fig. 10. Comparison of peak dilation angles under drained and undrained conditions.

6 Conclusions

A comprehensive database for investigating the shear strength and dilatancy is presented through a series of drained and undrained triaxial compression tests on calcareous sand from the South China Sea. It is observed that the peak strength is mobilized at an axial strain larger than that for most silica sands. The constant volume friction angle is measured as ~39°, which is higher than that of silica sand. The strength mobilization and volume change during shearing of calcareous sands are obviously different from those of silica sands, which requires particular concerns for offshore and coastal constructions in calcareous sand fields. According to the results of drained tests, Bolton (1986) equations can be used to describe the calcareous sands with slight particle breakage, although the fitting parameters Q, R and m need to be modified. An extensive comparison for calcareous

sands from a few onshore and offshore regions shows that the peak friction angle can be predicted reasonably well by Eq. (7). However, Eq. (7) may overestimate the peak friction angle if particle breakage is severe or the carbonate content of sand is low. The peak dilation angle of the South China Sea sand may be estimated by Eq. (8), although the equation does not perform as well for other calcareous sands. For the samples with relative density larger than 60%, the peak friction angles from the undrained tests tend to be slightly lower than those from the drained tests. It must be admitted that Eqs. (6)–(8) obtained in this paper are better to describe sand from the South China Sea. With differences in mineral composition and particle shape, the predictions for calcareous sands from other locations are with lower accuracy. In addition, Eqs. (6)–(8) are proposed based on the samples featured with slight particle breakage and further study is needed for calcareous sand with severe particle breakage.

Acknowledgrments

The calcareous sand sample was provided by Professor WANG Ren at Institute of Rock and Soil Mechanics, Chinese Academy of Sciences.

References

Airey, D.W., 1993. Triaxial testing of naturally cemented carbonate soil, *Journal of Geotechnical Engineering*, 119(9), 1379–1398.

Andersen, K.H. and Schjetne, K., 2013. Database of friction angles of sand and consolidation characteristics of sand, silt, and clay, *Journal of Geotechnical and Geoenvironmental Engineering*, 139(7), 1140–1155.

Baghdadi, Z.A., Ghazali, F.M. and Khan, A.M., 1991. Model pile testing in carbonate sediments of the Red Sea, *Canadian Geotechnical Journal*, 28(3), 423–433.

Been, K. and Jefferies, M., 2004. Stress–dilatancy in very loose sand, *Canadian Geotechnical Journal*, 41(5), 972–989.

Bolton, M.D., 1986. The strength and dilatancy of sands, *Géotechnique*, 36(1), 65–78.

Carraro, J.A.H., Prezzi, M. and Salgado, R., 2009. Shear strength and stiffness of sands containing plastic or nonplastic fines, *Journal of Geotechnical and Geoenvironmental Engineering*, 135(9), 1167–1178.

Cassidy, M.J., Airey, D.W. and Carter, J.P., 2005. Numerical modeling of circular footings subjected to monotonic inclined loading on uncemented and cemented calcareous sands, *Journal of Geotechnical and Geoenvironmental Engineering*, 131(1), 52–63.

Coop, M.R., 1990. The mechanics of uncemented carbonate sands, *Géotechnique*, 40(4), 607–626.

Coop, M.R. and Atkinson, J.H., 1993. The mechanics of cemented carbonate sands, *Géotechnique*, 43(1), 53–67.

Daouadji, A. and Hicher, P.Y., 2010. An enhanced constitutive model for crushable granular materials, *International Journal for Numerical and Analytical Methods in Geomechanics*, 34(6), 555–580.

Doherty, P., Spagnoli, G. and Bellato, D., 2016. Mixed-in-place response of two carbonate sands, *Proceedings of the Institution of Civil Engineers - Geotechnical Engineering*, 169(2), 153–163.

Erbrich, C.T., O'Neill, M.P., Clancy, P. and Randolph, M.K., 2010. Axial and lateral pile design in carbonate soils, in: Gourvenec, S. and White, D. (eds.), *Frontiers in Offshore Geotechnics II*, CRC Press, London, pp. 125–154.

Golightly, C.R. and Hyde, A.F.L., 1988. Some fundamental properties of carbonate sands, in: *Engineering for Carbonate Sediments*, Balkema, Rotterdam, pp. 69–78.

Guo, P.J. and Su, X.B., 2007. Shear strength, interparticle locking, and dilatancy of granular materials, *Canadian Geotechnical Journal*, 44(5), 579–591.

Hassanlourad, M., Salehzadeh, H. and Shahnazari, H., 2008. Dilation and particle breakage effects on the shear strength of calcareous sands based on energy aspects, *International Journal of Civil Engineering*, 6(2), 108–119.

He, S.H., Ding, Z., Xia, T.D., Zhou, W.H., Gan, X.L., Chen, Y.Z. and Xia, F., 2020. Long-term behaviour and degradation of calcareous sand under cyclic loading, *Engineering Geology*, 276, 105756.

Jafarian, Y., Javdanian, H. and Haddad, A., 2018. Dynamic properties of calcareous and siliceous sands under isotropic and anisotropic stress conditions, *Soils and Foundations*, 58(1), 172–184.

Jamiolkowski, M., Ghionna, V.N., Lancellotta, R. and Pasqualini, E., 1988. New correlations of penetration tests for design practice, *Proceedings of the 1st International Symposium on Penetration Testing*, Orlando, 263–296.

Jamiolkowski, M., Lo Presti, D.C.F. and Manassero, M., 2003. Evaluation of relative density and shear strength of sands from CPT and DMT, *Symposium on Soil Behavior and Soft Ground Construction Honoring Charles C. "Chuck" Ladd*, Cambridge, Massachusetts, United States.

Jensen, M.R., 2018. Shear strength parameters for Perth sands. *Engineering Research Project*, The University of Western Australia.

Kuwajima, K., Hyodo, M. and Hyde, A.F., 2009. Pile bearing capacity factors and soil crushabiity, *Journal of Geotechnical and Geoenvironmental Engineering*, 135(7), 901–913.

Lee, C.Y. and Poulos, H.G., 1991. Tests on model instrumented grouted piles in offshore calcareous soil, *Journal of Geotechnical Engineering*, 117(11), 1738–1753.

Lehane, B.M., Carraro, J.A.H., Boukpeti, N. and Elkhatib, S., 2014. Mechanical response of two carbonate sediments from Australia's North West Shelf, *Proceedings of the ASME 2014 33rd International Conference on Ocean, Offshore and Arctic Engineering*, San Francisco, California, USA.

Lehane, B.M., Schneider, J.A., Lim, J.K. and Mortara, G., 2012. Shaft friction from instrumented displacement piles in an uncemented calcareous sand, *Journal of Geotechnical and Geoenvironmental Engineering*, 138(11), 1357–1368.

Liu, Q.B. and Lehane, B.M., 2012. The influence of particle shape on the (centrifuge) cone penetration test (CPT) end resistance in uniformly graded granular soils, *Géotechnique*, 62(11), 973–984.

Lu, B., Li, G.X. and Huang, S.J., 2000. Acoustic-physical properties of calcareous seafloor soils and their significance in engineering geology, *China Ocean Engineering*, 14(3), 361–370.

Lv, Y.R., Li, X. and Wang, Y., 2020. Particle breakage of calcareous sand at high strain rates, *Powder Technology*, 366, 776–787.

Negussey, D., Wijewickreme, W.K.D. and Vaid, Y.P., 1988. Constant-volume friction angle of granular materials, *Canadian Geotechnical Journal*, 25(1), 50–55.

Porcino, D., Caridi, G. and Ghionna, V.N., 2008. Undrained monotonic and cyclic simple shear behaviour of carbonate sand, *Géotechnique*, 58(8), 635–644.

Rezvani, R., 2020. Shearing response of geotextile-reinforced calcareous soils using monotonic triaxial tests, *Marine Georesources & Geotechnology*, 38(2), 238–249.

Rui, S.J., Guo, Z., Si, T.L. and Li, Y.J., 2020. Effect of particle shape

on the liquefaction resistance of calcareous sands, *Soil Dynamics and Earthquake Engineering*, 137, 106302.

Salem, M., Elmamlouk, H. and Agaiby, S., 2013. Static and cyclic behavior of North Coast calcareous sand in Egypt, *Soil Dynamics and Earthquake Engineering*, 55, 83–91.

Salgado, R., Bandini, P. and Karim, A., 2000. Shear strength and stiffness of silty sand, *Journal of Geotechnical and Geoenvironmental Engineering*, 126(5), 451–462.

Sharma, S.S. and Ismail, M.A., 2006. Monotonic and cyclic behavior of two calcareous soils of different origins, *Journal of Geotechnical and Geoenvironmental Engineering*, 132(12), 1581–1591.

Teng, Y.N., Stanier, S.A. and Gourvenec, S.M., 2020. Mechanisms beneath rectangular shallow foundations on sands: vertical loading, *Géotechnique*, 70(12), 1083–1093.

Wang, G., Wang, Z.N., Ye, Q.G. and Wei, X., 2020. Particle breakage and deformation behavior of carbonate sand under drained and undrained triaxial compression, *International Journal of Geomechanics*, 20(3), 04020012.

Wang, G., Wang, Z.N., Ye, Q.G. and Zha, J.J., 2021. Particle breakage evolution of coral sand using triaxial compression tests, *Journal of Rock Mechanics and Geotechnical Engineering*, 13(2), 321–334.

Wang, X., Zhu, C.Q., Wang, X.Z. and Qin, Y., 2019. Study of dilatancy behaviors of calcareous soils in a triaxial test, *Marine Georesources & Geotechnology*, 37(9), 1057–1070.

Wang, X.Z., Jiao, Y.Y., Wang, R., Hu, M.J., Meng, Q.S. and Tan, F.Y., 2011. Engineering characteristics of the calcareous sand in Nansha Islands, South China Sea, *Engineering Geology*, 120(1-4), 40–47.

Wang, X.Z., Wang, X., Jin, Z.C., Meng, Q.S., Zhu, C.Q. and Wang, R., 2017. Shear characteristics of calcareous gravelly soil, *Bulletin of Engineering Geology and the Environment*, 76(2), 561–573.

White, D.J. and Bolton, M.D., 2004. Displacement and strain paths during plane-strain model pile installation in sand, *Géotechnique*, 54(6), 375–397.

Wu, Y., Cui, J., Li, N., Wang, X., Wu, Y.H. and Guo, S.Y., 2020. Experimental study on the mechanical behavior and particle breakage characteristics of hydraulic filled coral sand on a coral reef island in the South China Sea, *Rock and Soil Mechanics*, 41(10), 3181–3191. (in Chinese)

Xiao, P., Liu, H.L., Xiao, Y., Stuedlein, A.W. and Evans, T.M., 2018. Liquefaction resistance of bio-cemented calcareous sand, *Soil Dynamics and Earthquake Engineering*, 107, 9–19.

Zhang, J.R. and Luo, M.X., 2020. Dilatancy and critical state of calcareous sand incorporating particle breakage, *International Journal of Geomechanics*, 20(4), 04020030.